lubricants

MDPI

Article

Microstructure, Phase Components, and Tribological Properties of $Al_{65}Cu_{20}Fe_{15}$ Quasicrystal Coatings Deposited by HVOF

Sherzod Kurbanbekov [1,2], Tulkinzhon Gaipov [1,*], Pulat Saidakhmetov [3], Alibek Tazhibayev [4], Sherzod Ramankulov [1], Sattarbek Bekbayev [1], Arai Abdimutalip [1] and Dilnoza Baltabayeva [1]

[1] Department of Physics, International Kazakh-Turkish University Named H.A.Yasavi, Turkestan 161200, Kazakhstan; sherzod.kurbanbekov@ayu.edu.kz (S.K.); sherzod.ramankulov@ayu.edu.kz (S.R.); sattarbek.bekbayev@ayu.edu.kz (S.B.); aray.abdimutalip@ayu.edu.kz (A.A.); dilnoza.baltabayeva@ayu.edu.kz (D.B.)
[2] LLP "Institute of Innovative Technologies and New Materials", Turkestan 161200, Kazakhstan
[3] Department of Physics, M. Auezov South Kazakhstan University, Tauke Khan Ave. 5, Shymkent 160012, Kazakhstan; timpf_ukgu@mail.ru
[4] LLP "ALCOR", Almaty 050043, Kazakhstan; alibek@alcor.kz
* Correspondence: tulkinzhon.gaipov@ayu.edu.kz; Tel.: +7-7024962449

Abstract

Quasicrystalline coatings based on $Al_{65}Cu_{20}Fe_{15}$ are of increasing interest as potential alternatives to conventional wear-resistant materials due to their unique structural and tribological properties. This study explores the influence of air pressure during high-velocity oxy-fuel (HVOF) spraying on the phase composition, morphology, and wear behavior of $Al_{65}Cu_{20}Fe_{15}$ coatings deposited on U8G tool steel. Coatings were applied at a fixed spraying distance of 350 mm using three air pressures (1.9, 2.1, and 2.3 bar), with constant propane (2.0 bar) and oxygen (2.1 bar) supply. X-ray diffraction analysis identified the formation of $Al_{78}Cu_{48}Fe_{14}$ and $Al_{0.5}Fe_{1.5}$ phases, while scanning electron microscopy revealed a dense, uniform microstructure with low porosity and homogeneous element distribution across all samples. Tribological testing using the ball-on-disk method showed wear track widths ranging from 853.47 to 952.50 μm, depending on the air pressure applied. These findings demonstrate that fine-tuning the air pressure during HVOF spraying significantly influences the structural characteristics and wear resistance of the resulting quasicrystalline coatings, highlighting their promise for advanced surface engineering applications.

Keywords: $Al_{65}Cu_{20}Fe_{15}$; HVOF; U8G; tribology; microstructure; wear resistance

Received: 3 June 2025
Revised: 30 June 2025
Accepted: 3 July 2025
Published: 6 July 2025

Citation: Kurbanbekov, S.; Gaipov, T.; Saidakhmetov, P.; Tazhibayev, A.; Ramankulov, S.; Bekbayev, S.; Abdimutalip, A.; Baltabayeva, D. Microstructure, Phase Components, and Tribological Properties of $Al_{65}Cu_{20}Fe_{15}$ Quasicrystal Coatings Deposited by HVOF. *Lubricants* **2025**, *13*, 297. https://doi.org/10.3390/lubricants13070297

1. Introduction

One of the key challenges in modern materials science is the rapid degradation of surface layers due to intense wear, oxidation, and corrosion, especially under high-temperature and abrasive conditions [1–3]. To enhance resistance to these effects, high-performance hard coatings such as AlTiN [4], diamond-like carbon (DLC) [5], and ZrN [6] are widely applied, as they improve the mechanical properties. In addition, ceramic-metal composite coatings like WC-Co and Cr_3C_2-NiCr, known for their high hardness and wear resistance, are extensively used to protect working surfaces under severe operating conditions [7–9]. However, these coatings present several limitations, including brittleness, limited thermal stability, and the high cost of raw materials—particularly tungsten and cobalt—which restrict their broader industrial application [10,11]. A promising alternative is quasicrystalline coatings based on the Al–Cu–Fe system, which are characterized by high hardness,

low friction coefficient, excellent corrosion resistance, and thermal stability up to 800 °C. According to the literature, the microhardness of such coatings typically ranges from 700 to 1500 HV, while the coefficient of friction may vary within the range of 0.05 to 0.8, depending on the coating deposition conditions and testing environment. Such coatings hold promise for applications in the aerospace industry, energy sector, and mechanical engineering, where long-term surface protection is required under harsh operating conditions [12–15]. A key advantage of these coatings is their compatibility with various deposition methods, including thermal spraying, laser and plasma deposition, as well as the most efficient technique—HVOF [16–19].

The HVOF method is one of the most effective and versatile coating techniques for various industrial applications. Such coatings are widely used in industries where equipment operates under extreme conditions: high pressure, chemical exposure, and elevated temperatures, providing reliable protection and extending the service life of components. Due to the minimal substrate heating and high particle velocity, the HVOF process reduces thermal stresses and minimizes the risk of coating deformation and cracking [20]. The key advantage of the method is the ability to use various types of ceramic and carbide powders, which broadens its range of applications [21]. Coatings produced by HVOF retain excellent mechanical properties even at elevated temperatures and making them suitable for use in environments with thermal fluctuations. Additionally, the method allows coatings to be applied to surfaces with complex geometries, including pipelines, shafts, axles, and other components. This, in turn, can be an effective solution for the repair and restoration of worn components [22].

HVOF spraying, with heating temperatures reaching up to 3000 °C, is particularly effective for applying quasicrystalline coatings based on $Al_{65}Cu_{20}Fe_{15}$. At high temperatures, the powder particles form coatings that retain their quasicrystalline structure with minimal phase changes, and the resulting coatings can achieve a coefficient of friction of approximately 0.1 under dry sliding conditions [23]. The high particle velocity of up to 700 m/s ensures limited contact with oxygen, which helps prevent excessive oxidation, as confirmed by $Al_{65}Co_{18}Cu_{17}$ (d-QC) quasicrystalline coatings deposited by HVOF at an oxygen-to-kerosene (O/K) stoichiometry ratio of 1.04, where oxidation was effectively minimized [24]. Since quasicrystalline powder is sensitive to overheating, the HVOF method provides better preservation of the phase composition compared to plasma spraying. Another key advantage of this method is its low thermal impact, as the substrate temperature during deposition does not exceed 100–200 °C, thereby preventing deformation and structural changes [25].

The purpose of this article is to investigate the process of depositing $Al_{65}Cu_{20}Fe_{15}$ quasicrystalline coatings on the surface of U8G steel using the HVOF spraying method, followed by a detailed analysis of their microstructure, phase composition, and tribological properties. Particular attention is focused on evaluating the wear resistance and friction behavior of the coatings in order to determine their suitability for use in components of aerospace, automotive, and mechanical engineering systems that operate under conditions of high mechanical stress and intense friction.

2. Materials and Methods

The research was conducted on coating samples applied to the outer surface of U8G (the composition is shown in Table 1) tool carbon steel substrates, which comply with GOST 1435-99 standards [26]. The thickness of the substrates was 7 mm, with width and length dimensions of 20 × 20 mm. The coatings were deposited using the HVOF spraying technique with a Termika-3 installation (Saint Petersburg, Russia). The diagram of the device for the HVOF spraying process, the plasmatron, is shown in Figure 1.

Table 1. Chemical properties of U8G steel.

Element	C	Si	Mn	Ni	S	P	Cr	Cu	Fe
Mass fraction, %	0.81–0.89	0.17–0.33	0.33–0.58	up to 0.25	up to 0.028	up to 0.03	up to 0.2	up to 0.25	~97

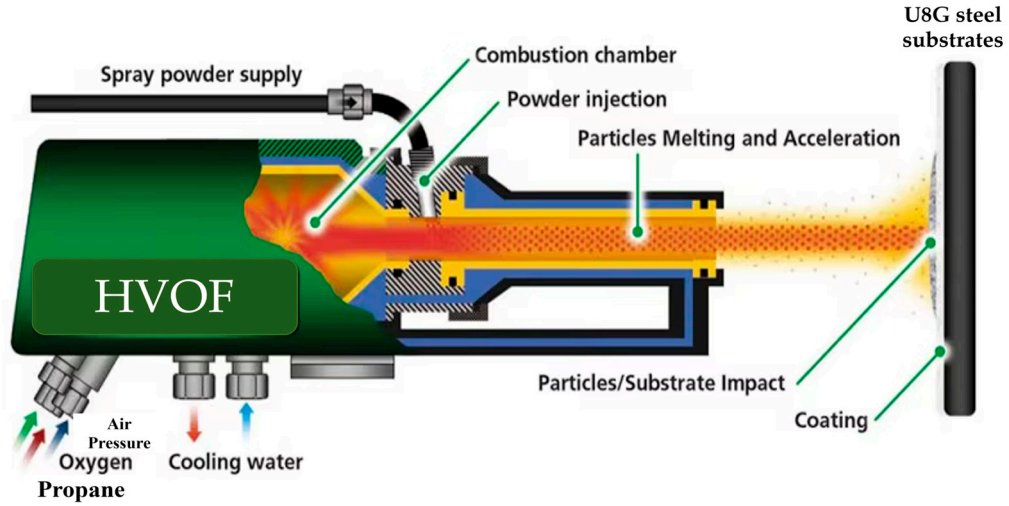

Figure 1. HVOF spraying process.

Quasicrystalline material Al-Cu-Fe, consisting of aluminum (Al)–65 at.%, copper (Cu)–20 at.%, and iron (Fe)–15 at.%, ground into fine powder, was heated and directed onto the substrate, forming a coating. The particle size of the resulting powders ranged from 60 to 80 µm, ensuring efficient spraying (Figure 2).

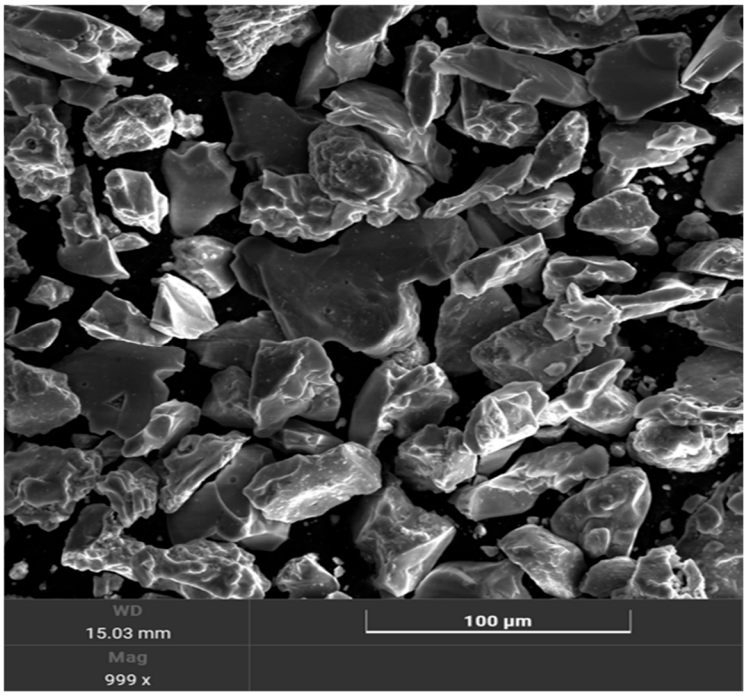

Figure 2. Powder particle size before coating deposition.

In this study, special attention is given to the variation of air pressure during HVOF spraying, as this parameter plays a crucial role in controlling particle acceleration, temperature distribution, and the degree of oxidation during coating formation. The experiment was repeated three times. Air pressure directly affects the velocity and structure of the

gas flow, which in turn determines the melting degree of the particles and the nature of their impact on the substrate. To accurately assess the influence of air pressure alone, all other parameters—such as spraying distance (350 mm), propane pressure (2 bar), and oxygen pressure (2.1 bar)—were kept constant. In our previous theoretical study [20], it was found that this approach enables the establishment of stable thermal and kinetic conditions, ensuring an accurate evaluation of the effect of a single variable. In this study, the spraying parameters were selected based on the technological characteristics of the HVOF process and the physical principles of forming high-quality coatings. The nozzle-to-substrate distance of 350 mm was chosen to ensure the optimal temperature and particle velocity, preventing overheating and preserving the quasicrystalline structure. The propane pressure of 2 bar was set to maintain a stable flame, which is necessary for uniform particle heating without complete melting. The air pressure, ranging from 1.9 to 2.3 bar, was used to control the kinetic energy of the particles and to optimize coating density and adhesion. The oxygen pressure of 2.1 bar ensured stable and complete fuel combustion, minimizing the risk of particle oxidation during transport. All parameters were carefully selected to maintain spraying stability, achieve high coating quality, and avoid thermal degradation of the material. This enhances the reliability of the results and supports the identification of optimal process conditions for producing dense, uniform, and wear-resistant quasicrystalline coatings; the regimes are shown in Table 2. Due to the selected particle size and spraying distance, the dwell time of the powder in the flame was sufficient for complete heating and for reaching the substrate with the necessary energy, which was confirmed by the uniformity of the deposited coating. Preservation of the quasicrystalline structure of the material was achieved by controlling temperature and velocity, thereby preventing overheating and the degradation of the powder's unique properties.

Table 2. HVOF spraying parameters for quasicrystalline coatings.

Sample	Nozzle-to-Substrate Distance (mm)	Propane Pressure (bar)	Air Pressure (bar)	Oxygen Pressure (bar)
Sample a	350	2	2.1	2.1
Sample b	350	2	2.3	2.1
Sample c	350	2	1.9	2.1

To examine the sample with high precision and obtain detailed surface images, a Tescan Vega 4 SEM (Brno, Czech Republic) with a thermionic tungsten cathode was used. One of the key advantages of this method is the ability to analyze coating adhesion and identify defects. To determine the chemical composition of the $Al_{65}Cu_{20}Fe_{15}$ powder, the working distance of the SEM was set at 10–15 mm, and the acceleration voltage was increased to 25 kV, and different types of detectors were used: EDS to identify the elements present in the sample and their concentrations; BSE (Backscattered Electron Detector) to visualize compositional differences in the material; and SE (Secondary Electron Detector) to provide high-resolution surface imaging, enabling the research of topography and fine structural details.

The magnification was increased up to 999×, with a penetration depth of 0.5–3 μm. Additionally, SEM images were combined with X-ray diffraction (XRD) data, providing a comprehensive analysis of the coating structure.

The phase composition of the coatings was analyzed using XRD with the XPERT-PRO diffractometer from Panalytical (Philips Corporation, Amsterdam, The Netherlands). The device was equipped with a copper anode (Cu) and a Kα X-ray source with a wavelength of 1.5406 Å. The studies were conducted at a temperature of 25 °C, an operating voltage of

40 kV, and a current of 30 mA. Scanning was performed over an angular range of 20.01° to 89.99°, with a step size of 0.02°, and the data acquisition time for each measurement was 2 seconds. The collected data were processed using the HighScore Plus software package (Malvern Panalytical—"HighScore Plus | XRD Analysis Software", 4 July 2025).

Tribological tests were performed using a TRB3 tribometer (Anton Paar, Buchs, Switzerland) to evaluate the wear resistance, friction coefficient, and durability of the coatings. The experiments were conducted in accordance with the ASTM G99 standard (Standard Test Method for Wear Testing with a Pin-on-Disk Apparatus) [27]. A 100Cr6 steel ball with a diameter of 3 mm served as the counter body, and a constant normal load of 5 N was applied. The ball moved along a unidirectional circular path with a wear track diameter of 90 mm and a sliding radius of 3 mm. The linear sliding speed was 5 cm/s, corresponding to a rotational speed of 159.15 rpm. Each test was carried out for 30 min under ambient conditions, with the relative humidity maintained at 29%. Throughout the tests, the coefficient of friction was continuously recorded. The initial Hertzian contact pressure was calculated using Hertzian contact theory, resulting in a maximum contact pressure of approximately 1.67 GPa for the applied load and ball radius. The reduced elastic modulus, accounting for the elastic properties of the 100Cr6 steel ball and the Al-Cu-Fe quasicrystalline coating, was determined to be 104.1 GPa. The applied load was selected in accordance with the ASTM G99 standard to ensure sufficient contact stress while avoiding premature coating failure. Data processing and tribological performance analysis were conducted using Origin software (OriginLab Corporation, Northampton, MA, USA). Available online: www.originlab.com (accessed on 4 July 2025).

The microhardness of $Al_{65}Cu_{20}Fe_{15}$ based quasicrystalline coatings obtained by the HVOF method was investigated using an HLV-1DT Vickers microhardness tester with a touch screen (Shanghai Hualong Test Instruments Corporation, Shanghai, China). The test load was 0.2 N, and the dwell time was 10 seconds. The measured microhardness values ranged from 730 to 800 HV. This study allows for a deeper analysis of the mechanical properties of the obtained coatings and an assessment of their performance. The high microhardness values indicate the high hardness and strength of the quasicrystalline coatings, which positively affect their wear resistance and long-term durability. In addition, the structural stability and strength of the coatings obtained by the HVOF method demonstrate their high potential for widespread industrial application.

3. Results and Discussion

3.1. Morphology of the Coatings

The morphology of the coatings formed under different air pressure conditions (2.1, 2.3, and 1.9 bar) at a constant spraying distance of 350 mm reveals significant variations in layer structure and density. These differences are illustrated in Figure 3, which presents SEM images of the samples deposited at each respective air pressure. As shown in Figure 3a, at an air pressure of 2.1 bar, the coating surface exhibits moderately developed topography with pronounced porosity and areas containing microscopic depressions and densifications. The structure appears heterogeneous: bright zones are associated with regions enriched in heavier elements (possibly iron from the substrate or AlFe phases), whereas darker regions may correspond to areas with higher aluminum content or less dense quasicrystalline particles. This heterogeneity may be attributed to uneven recrystallization caused by high-velocity particle impact on the substrate, as well as thickness variations within the coating layer. Figure 3b shows the morphology of the coating obtained at an increased air pressure of 2.3 bar. It is evident that at this spraying regime, the most dense and uniform structure is formed, characterized by minimal porosity and good particle sintering. It has been established that the formation of such a morphology is determined by the critical im-

portance of spraying process parameters, as demonstrated in the work of Karpov et al. [28]. A significant number of rounded and closely packed particles is also observed, indicating intensive melting of the powder under the given conditions. Distinct bright regions suggest the possible formation of intermetallic phase fragments or enhanced diffusion of copper and iron into the aluminum matrix, as reported in the study by Chugunova et al. [29], which corresponds to the conditions of thermal activation at this spraying mode. It is likely that the structure of the quasicrystalline powder, under high collision energy, contributed to the formation of ordered yet amorphous-like zones, typical of quasicrystals. In Figure 3c, where the air pressure was 1.9 bar, the coating structure becomes more porous, with an increased number of microvoids and irregularly shaped particles. As can be seen, there is also a decrease in the contrast between the phases, which may be attributed to insufficient particle melting and weak adhesion to the substrate. Possibly, the lower kinetic energy of particles at reduced air pressure does not provide adequate compaction and uniform stacking of the coating material. As a result, structural defects appear, compromising the integrity of the protective layer.

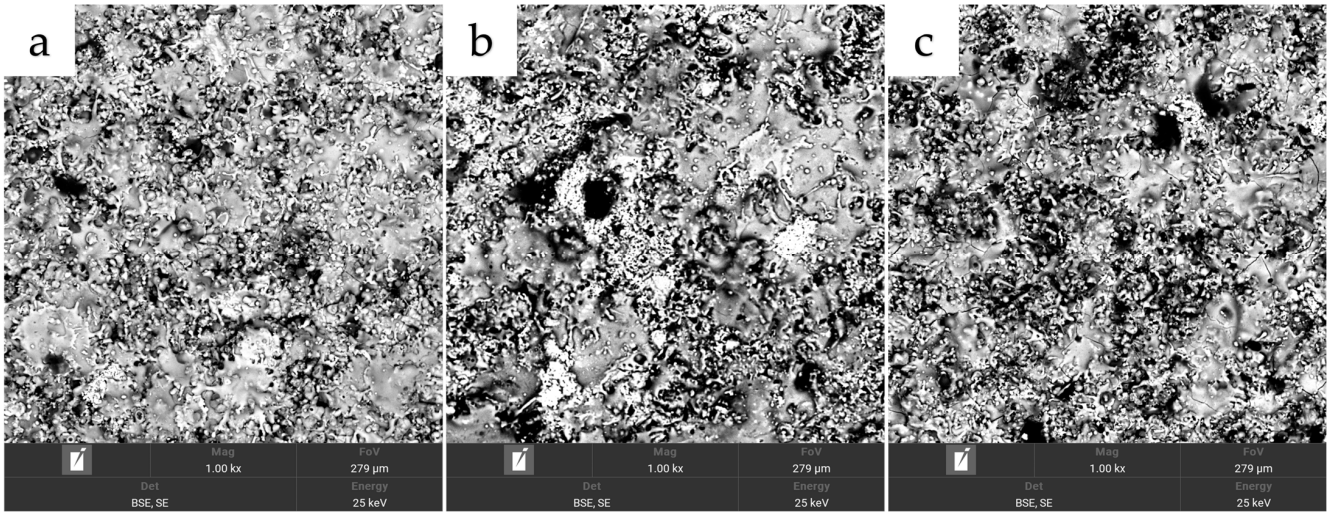

Figure 3. Surface morphology of the coatings: (**a**) 2.1 bar, (**b**) 2.3 bar, (**c**) 1.9 bar.

The surface morphology of the $Al_{65}Cu_{20}Fe_{15}$ quasicrystalline coatings observed in electron microscope images indicates differences in density and porosity, which are attributed to variations in the HVOF process parameters. To gain a deeper understanding of the structure formation mechanisms, a microstructural evaluation of the coating cross-sections was carried out under different air flow conditions, as shown in Figure 4.

As shown in Figure 4a, the coating exhibits a relatively continuous structure with moderate density and a thickness ranging from 33.2 to 33.6 µm. The interface with the steel substrate is clearly defined but displays slight waviness and minor porosity. This morphology may be attributed to the balanced kinetic energy of the particles, where partial melting and deformation upon impact promote adhesion and compaction. However, incomplete filling of microvoids may result in localized inhomogeneities, potentially influenced by the nonequilibrium solidification behavior of the quasicrystalline powder. The two-tone contrast observed in the BSE image indicates compositional differences, likely reflecting phase separation between aluminum-rich and iron/copper-rich domains. Figure 4b corresponds to the highest air pressure (2.3 bar), under which the coating develops an optimal structure with densely packed particles, minimal porosity, and a continuous layer. The coating thickness varies from 23.5 to 31.8 µm. Increased air pressure enhances the acceleration of powder particles, resulting in greater deformation, spreading, and fusion upon impact, which contributes to the formation of a more uniform coating.

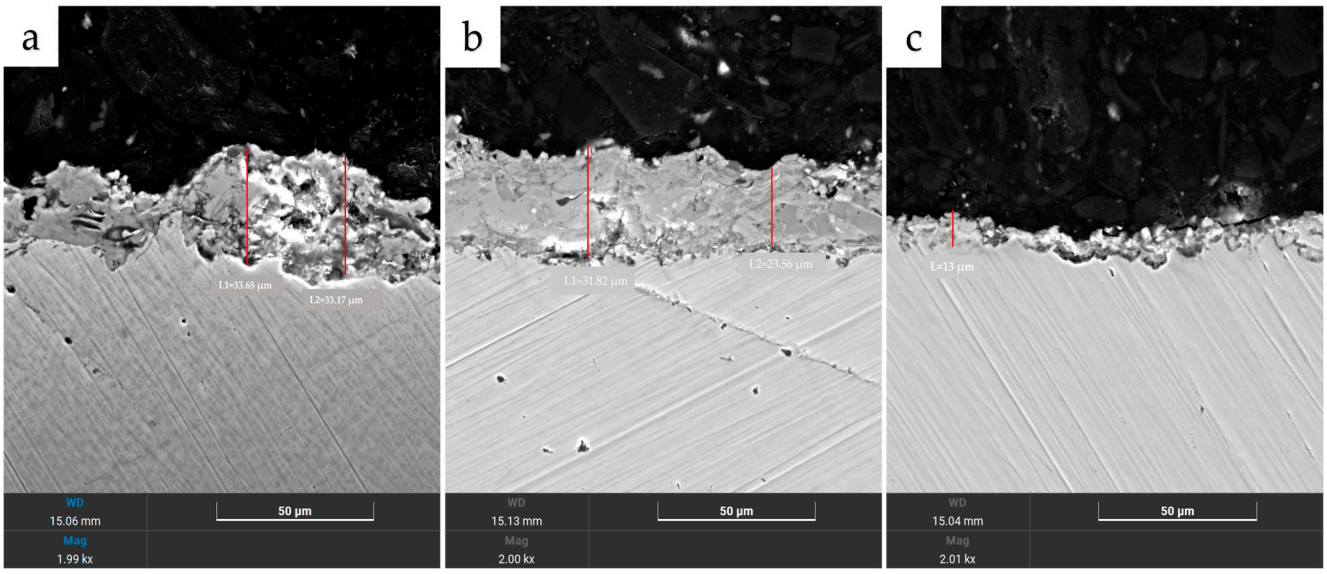

Figure 4. SEM cross-sectional image of samples with a quasicrystalline coating based on $Al_{65}Cu_{20}Fe_{15}$: (**a**) 2.1 bar, (**b**) 2.3 bar, (**c**) 1.9 bar.

The observed fine-grained texture indicates intensive mechanical interlocking and thermal softening during the deposition process, which is consistent with the findings reported by Wang et al. [30]. This type of structure likely contributes to enhanced wear resistance and slows crack propagation due to the absence of gaps between particles and strong cohesion. In contrast, Figure 4c shows the coating formed under reduced air pressure (1.9 bar), which is characterized by insufficient density and decreased thickness (~13 µm). The lower particle velocity limits the thermal and kinetic energy upon impact, resulting in poor spreading and partial bonding. As a result, the structure appears porous, with visible voids and weak adhesion to the substrate. This may lead to the deterioration of mechanical properties and reduced stability under tribological stress. The dark gray areas observed in the BSE image indicate inhomogeneity and potential phase separation, likely due to incomplete melting of $Al_{65}Cu_{20}Fe_{15}$ particles.

The morphological features revealed during the microstructural analysis of $Al_{65}Cu_{20}Fe_{15}$ coatings deposited by the HVOF method indicate significant differences in density, porosity, and particle packing uniformity depending on the air supply regime.

3.2. EDS Line Scanning

To gain a deeper understanding of the nature of these variations, an analysis of the chemical element distribution across the coating's cross-section was conducted using EDS line scanning. The results are presented in Figure 5 for the samples obtained at air pressures of 2.1, 2.3, and 1.9 bar, respectively. As shown in Figure 5a, the distribution graph reveals that the most prominent peaks correspond to aluminum (Al K$\alpha \approx 1.49$ keV) and iron (Fe K$\alpha \approx 6.4$ keV), reflecting the base composition of the quasicrystalline powder. A stable presence of copper (Cu K$\alpha \approx 8.04$ keV) is observed, with a relatively smooth decline in intensity near the coating–substrate interface. This indicates a fairly uniform distribution of Cu throughout the coating, presumably in the form of a solid solution or Al_2Cu phase, as explained by Suárez et al. [31]. A significant increase in Fe signal intensity near the substrate interface suggests diffusion of iron from the U8G steel substrate into the coating region. This supports the possible formation of intermetallic phases such as $AlFe_3$ or AlFe, which aligns with the densified zones observed in the microstructure, as noted in the study by Huttunen et al. [32]. The oxygen signal intensity (O K$\alpha \approx 0.52$ keV) remains moderate, indicating its unavoidable presence in the HVOF process, though it is minimized. The

most compact and homogeneous coating was observed at an air pressure of 2.3 bar, as shown in Figure 5b. It is evident that the line profiles of all major elements—Al, Cu, Fe, and O—display clear plateaus within the coating region and sharp drops at the interface with the substrate, indicating good layer integrity and minimal element diffusion into the substrate. This may be attributed to the high combustion temperature of the oxygen–fuel mixture in the flame zone and the increased air flow, which promotes the accelerated ejection of particles and creates optimal conditions for partial melting of the quasicrystalline powder. The particularly uniform distribution of Cu indicates the presence of a stable AlCuFe quasicrystalline phase, resistant to high-energy impact. The strong Al signal and the characteristic shape of its curve suggest the dominance of an aluminum matrix, possibly in the form of β-Al (Cu, Fe), as reported by Laijun et al. [33]. A sharp increase in Fe content near the substrate interface confirms the formation of a transition zone, likely associated with mechanochemical interactions. The measured energy peak values correspond well with tabulated characteristic values [Al Kα ≈ 1.49 keV; Fe Kα ≈ 6.40 keV; Cu Kα ≈ 8.04 keV], as presented by Rukdee et al. [34]. The dominance of Al peak intensity over Fe and Cu (Al > Fe > Cu) further indicates aluminum prevalence in the coating composition. Under reduced air pressure, as shown in Figure 5c, a less uniform elemental distribution is observed. The Al intensity curve exhibits strong fluctuations instead of a plateau, which suggests the presence of voids or porosity in the structure. This may result from partial particle coalescence and insufficient powder melting. An abnormally high local Cu peak is also recorded, potentially indicating uneven evaporation or secondary oxidation of copper (e.g., formation of Cu_2O or CuO, with a slightly increased O peak at 0.52 keV). The Fe peaks are less clearly localized, pointing to a diffuse interface and potentially unstable coating adhesion. The presence of oxygen, distributed chaotically, confirms the existence of oxidized regions along particle boundaries.

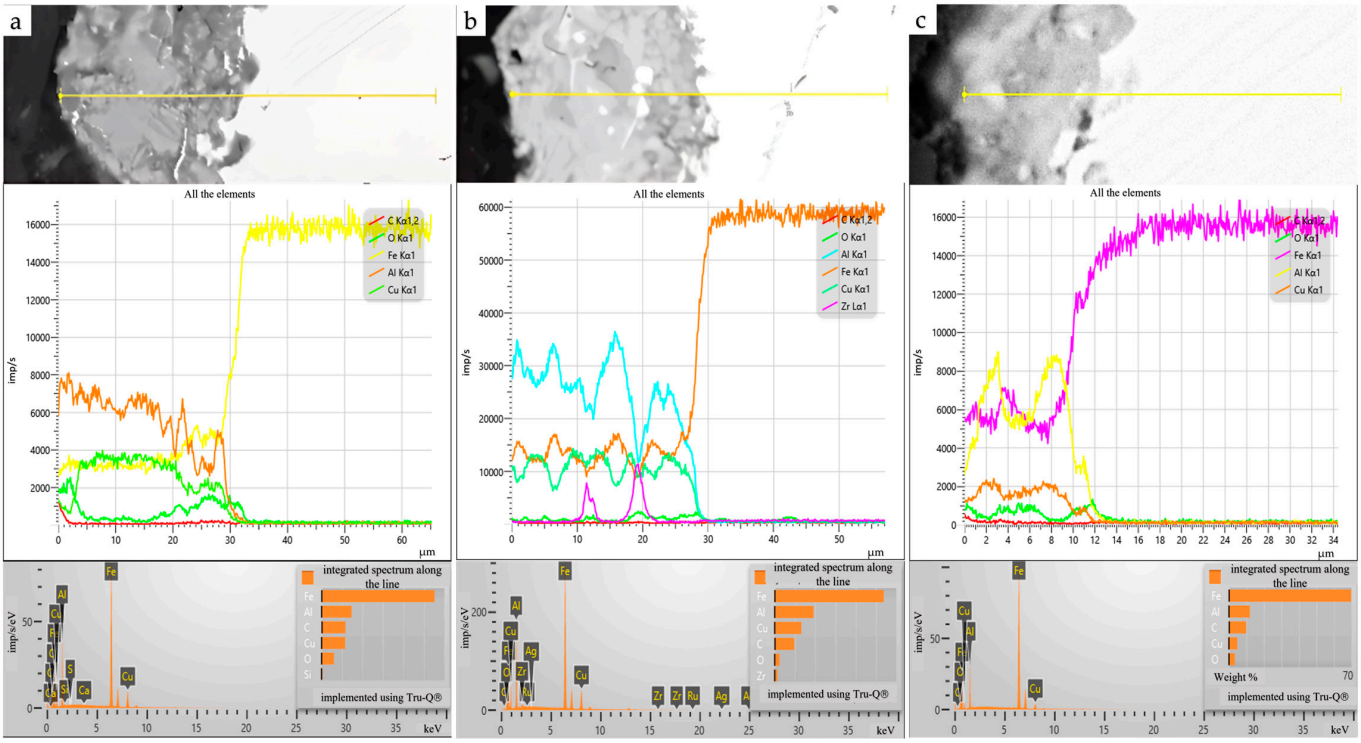

Figure 5. SEM images with EDS line scan paths across the cross-sections of three samples with $Al_{65}Cu_{20}Fe_{15}$ quasicrystalline coatings deposited by the HVOF method. (**a**) 2.1 bar, (**b**) 2.3 bar, (**c**) 1.9 bar.

3.3. Point Analysis of the Coating Cross-Sections and E-Mapping Analysis

In addition, a point analysis of the coating cross-sections was carried out, and the results are presented in Figure 6. In the SE images (top row), the selected areas for EDS measurements are shown. Spectrum 2 was selected for samples a and c, and spectrum 8 for sample b, as they correspond more closely to the expected composition of the $Al_{65}Cu_{20}Fe_{20}$ quasicrystalline alloy.

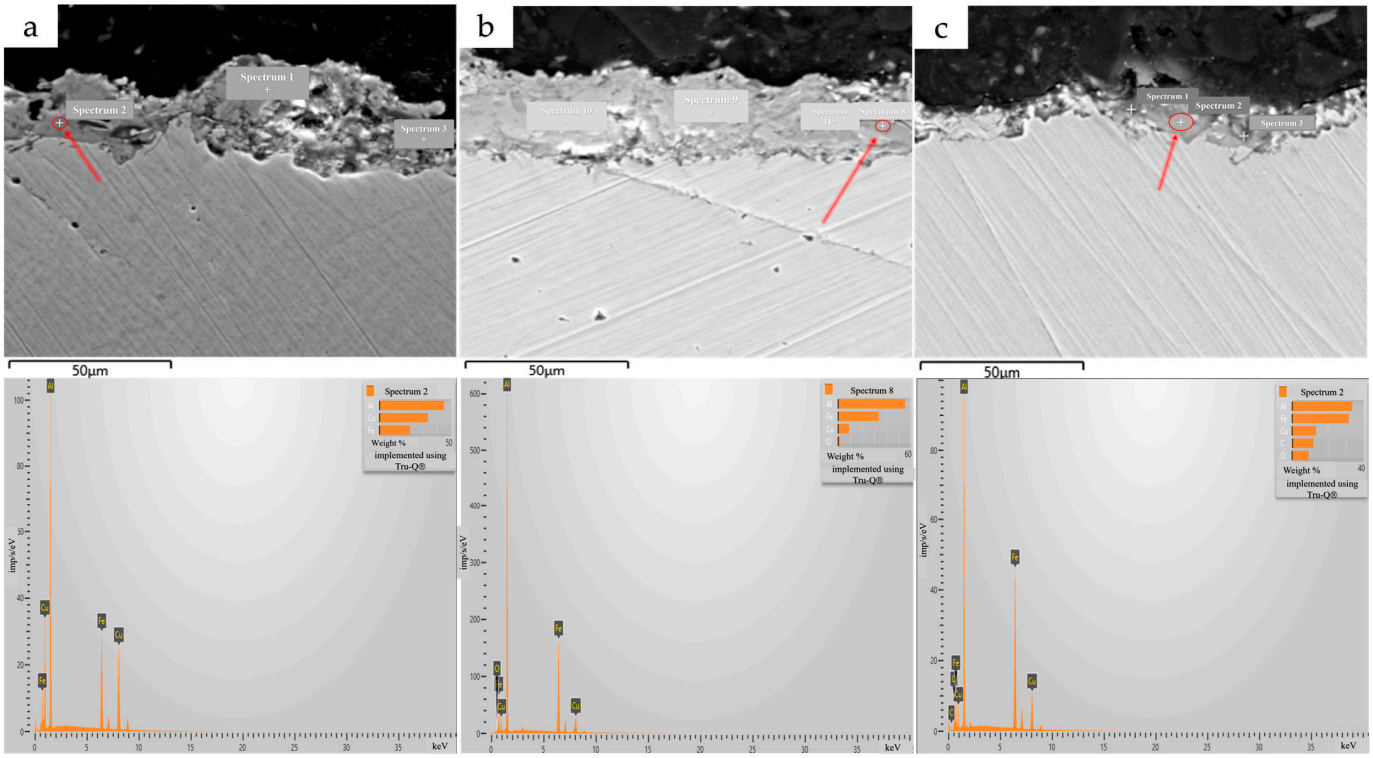

Figure 6. Microstructure of the coating applied to the substrate, showing the marked EDS analysis points (Spectrum 2, Spectrum 8, Spectrum 2): (**a**) 2.1 bar, (**b**) 2.3 bar, (**c**) 1.9 bar.

The corresponding spectra and quantitative elemental composition (bottom row) confirm the presence of aluminum, copper, and iron as the main constituents of the coating. The obtained data indicate chemical stability and homogeneity within the analyzed regions. Minor differences in the intensity of elemental peaks may be attributed to local structural variations in the coating or to deposition dynamics under different spraying conditions. Overall, the results confirm that the applied technological parameters enable the successful formation of quasicrystalline coatings with the desired elemental composition. Table 3 presents the elemental composition (wt.%) of the coatings based on point EDS analysis from Figure 6. The reference composition of the quasicrystalline i-phase in the Al-Cu-Fe system, according to Shalaeva and other authors [35], closely corresponds to the values obtained in our point EDS analysis. The stable single-phase structure $Al_{62.4}Cu_{25.3}Fe_{12.3}$, identified by electron microprobe analysis in this study, confirms the characteristic compositional range associated with icosahedral quasicrystalline ordering.

Table 3. Atomic percentages of elements in different samples detected in the spectra.

№	Al	Cu	Fe	O	C
Sample a	55.63	9.06	33.66	1.65	-
Sample b	33.65	13.34	31.68	1.12	20.21
Sample c	45.00	33.73	21.27	-	-

All measured spectra also confirmed the presence of aluminum, copper, and iron—the main elements of the Al-Cu-Fe system. The elemental ratios obtained from the spectra correspond to the typical composition of the stable icosahedral quasicrystalline phase (i-phase), previously reported in cast Al-Cu-Fe alloys by Chugunov et al. [29], where Al ≈ 60–63 at.%, Cu ≈ 24–27 at.%, and Fe ≈ 11–13 at.%.

Figure 7 shows SEM images with maps of the distribution of cross-sectional elements of Al-Cu-Fe coatings after application by the HVOF method. It is evident from Figure 7a that the coating exhibits a high concentration of copper (Cu) and oxygen (O), whereas aluminum (Al) is present only in isolated areas. This distribution may be explained by the reduced collision energy of particles (compared to the 2.3 bar regime), where aluminum particles, due to their low density and high reactivity, may undergo partial oxidation in-flight and fail to incorporate sufficiently into the coating. The dominance of oxygen may be associated with the formation of surface CuO phases, as well as with the lower particle density of the coating, which promotes more intense oxidation reactions with the surrounding atmosphere. The deficiency of aluminum may also indicate partial loss of its fraction in the form of volatile or oxidized species during powder transport to the substrate. In Figure 7b, the most balanced and dense coating is observed, with aluminum prevailing throughout the layer thickness and copper localized in distinct regions. This morphology suggests more complete particle melting, improved adhesion, and enhanced reactivity of aluminum at high temperatures and impact energy, as demonstrated in the study by Huttunen-Saarivirta et al. [32].

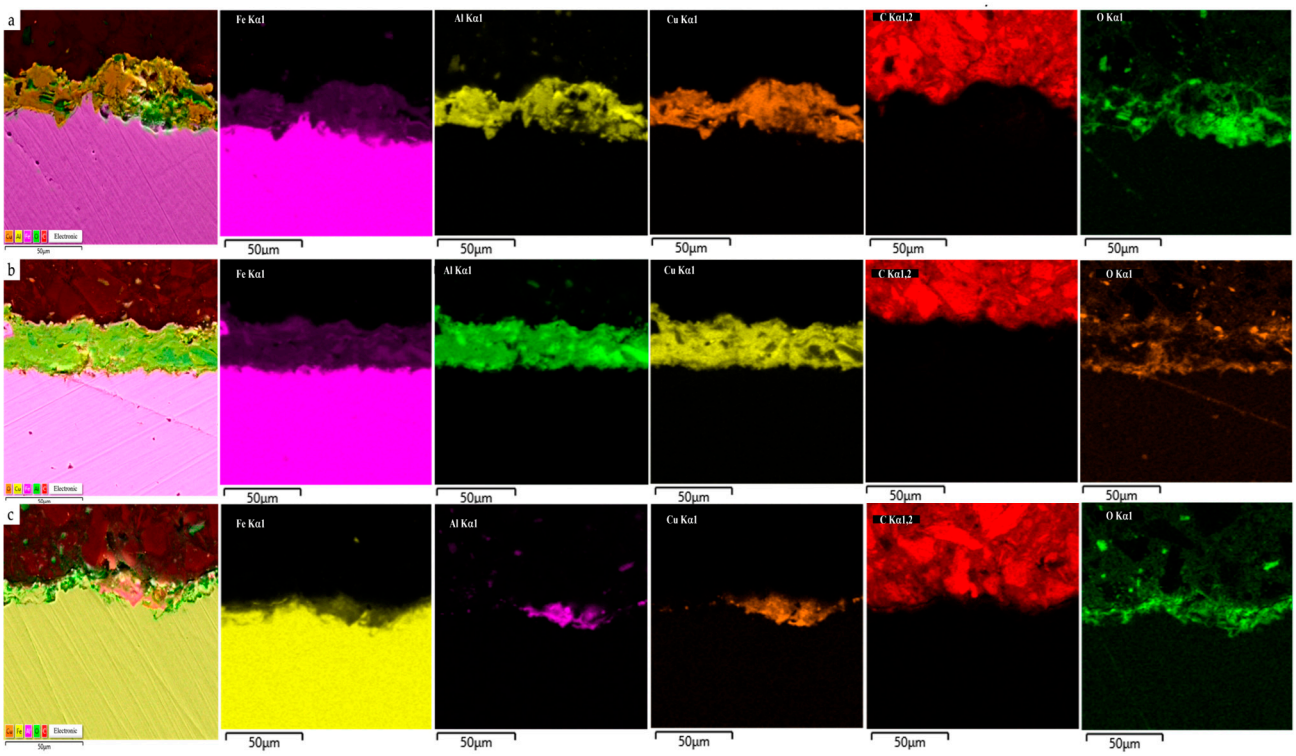

Figure 7. Elemental distribution maps of the sample cross-sections obtained by EDS analysis. (**a**) 2.1 bar, (**b**) 2.3 bar, (**c**) 1.9 bar.

In Figure 7c, the coating exhibits an increased concentration of iron (Fe) in the upper region, along with a notable presence of oxygen (O). Aluminum and copper are localized in isolated, uneven regions, indicating insufficient temperature and kinetic energy of the particles. As a result, the $Al_{65}Cu_{20}Fe_{15}$ quasicrystalline powder particles do not fully melt, and their impact on the substrate fails to ensure proper densification. Iron may have

partially migrated from the substrate into the coating due to weak impact bonding and/or a rebonding effect. Additionally, fragments of intermetallic compounds may form, as described by Tan et al. [36]. The high oxygen content may indicate the formation of iron oxides (Fe_2O_3, Fe_3O_4) and aluminum oxides in the upper layer, particularly in porous or weakly compacted regions. The low aluminum content in the coating zone could also result from its insufficient in-flight energy and failure to integrate into the coating structure, especially due to material loss during transport. Conversely, a high aluminum concentration may be associated with deeper penetration into the coating or the possible formation of intermetallic phases such as Al-Fe and Al-Cu. The moderate presence of Cu may suggest phase separation during solidification—copper partially concentrates in localized areas, being unevenly distributed across the matrix, as noted by Babilas et al. [37]. The formation of a reaction zone is evidenced by the upward diffusion of Fe and partial downward penetration of Al, indicating intense diffusion under high-energy deposition conditions.

3.4. XRD Analysis

Based on XRD analysis and its correlation with experimental results, the phase composition of the sprayed coatings was determined, as demonstrated in Figure 8. According to the XRD data, after deposition of the quasicrystalline coating by HVOF spraying using propane, oxygen, and air, the phases $Al_{0.5}Fe_{1.5}$ and $Al_{78}Cu_{48}Fe_{14}$ were identified in the samples. As observed in the diffraction patterns, with changes in spraying parameters, the intensity of the peaks corresponding to the $Al_{0.5}Fe_{1.5}$ phase gradually decreases, while the intensity of the quasicrystalline phase peaks increases. All quasicrystals are inherently classified as complex structures due to the absence of translational periodicity and the virtually unlimited size of their unit cells. In terms of structural complexity, the quasicrystalline phases are followed by closely related but fully crystalline approximant phases (AC) [38]. The intermetallic compound $Al_{0.5}Fe_{1.5}$ is an ordered solid phase in the Fe-Al system containing approximately 25 at.% aluminum. At room temperature, this compound exhibits a cubic DO_3-type structure with a space group Im-3m and a lattice parameter of about a = 2.91 Å [39,40]. The DO_3 structure is characterized by an ordered arrangement of Fe and Al atoms, which significantly enhances the hardness and stability of the material compared to conventional solid solutions in the Fe-Al system. In terms of tribological properties, $Al_{0.5}Fe_{1.5}$ coatings deposited by the HVOF method demonstrate a relatively high coefficient of friction ($\mu \approx 0.6$–0.7) under dry sliding conditions against hard materials such as steel [41]. The elevated friction coefficient is mainly attributed to the metallic nature of the intermetallic compound and the adhesive nature of surface contact during friction. During wear testing, $Al_{0.5}Fe_{1.5}$ coatings predominantly exhibit adhesive-abrasive wear mechanisms accompanied by the formation of microcracks. Despite its high hardness, the intermetallic phase possesses moderate brittleness, which contributes to crack formation and chipping under mechanical loading. The identified $Al_{78}Cu_{48}Fe_{14}$ phase is characterized by a cubic crystal structure with space group Pm-3 and a unit cell parameter of a = 12.3120 Å, indicating a complex atomic packing typical of ordered intermetallics in the Al-Cu-Fe system. A transition from sample a to samples b and c is accompanied by a decrease in the intensity of $Al_{78}Cu_{48}Fe_{14}$ quasicrystalline phase peaks and a relative increase in the intensity of peaks of the intermetallic $Al_{0.5}Fe_{1.5}$ phase. This indicates a reduction in the quasicrystalline phase content in the coating structure as the spraying conditions are varied.

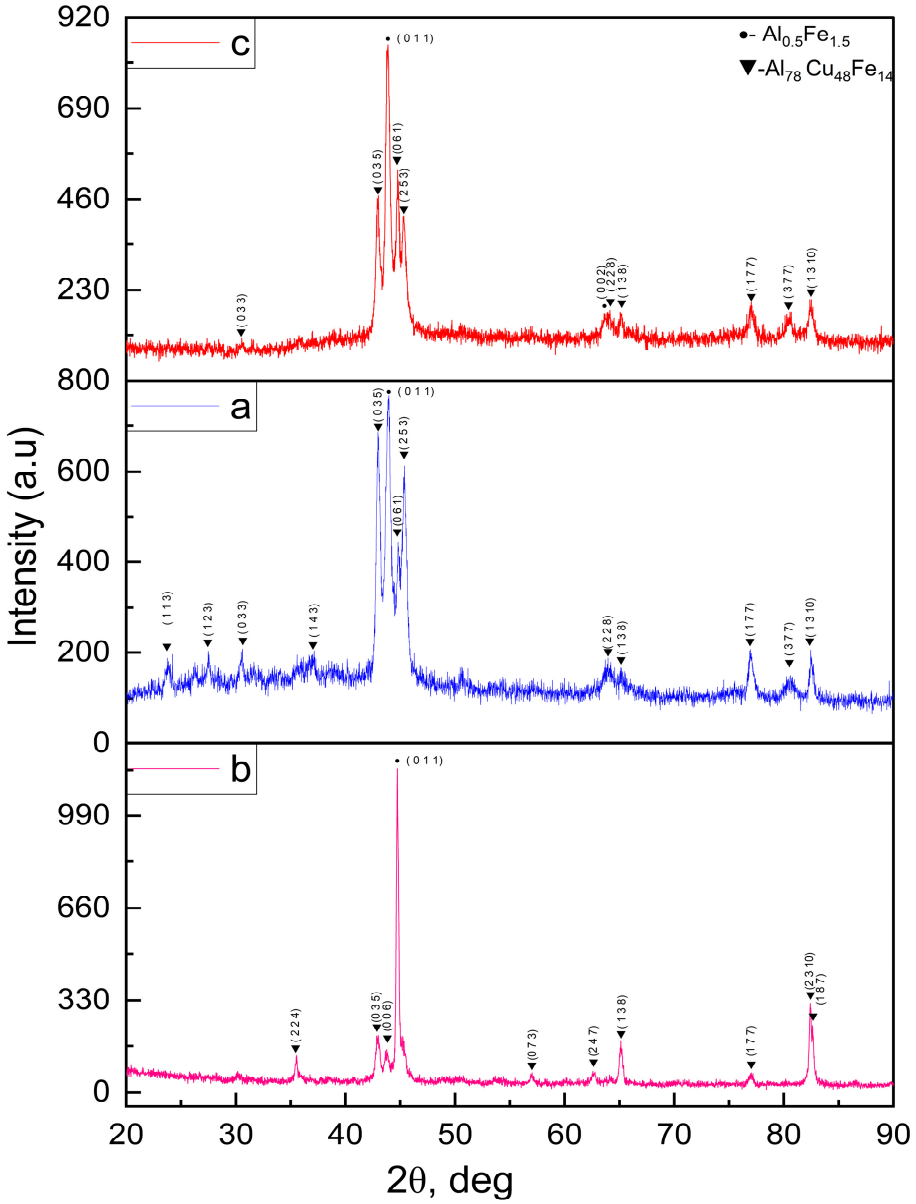

Figure 8. The X-ray analysis of U8G steel after coating with $Al_{65}Cu_{20}Fe_{15}$ under different HVOF spraying conditions. (**a**) 2.1 bar, (**b**) 2.3 bar, (**c**) 1.9 bar.

3.5. Tribological Performance

3.5.1. Friction Coefficient

The evolution of the friction coefficient (μ) during sliding reveals significant differences in the tribological behavior of the three coating samples, as demonstrated in Figure 9. In the third sample 9c, the friction coefficient after the ball adaptation period was 0.8; in the first sample 9a, it was 0.87; and in the second sample 9b, it was 0.9. As shown in Figure 8, no significant changes were observed in samples a and c after the initial stage, while sample b exhibited a decrease in the friction coefficient. On sample a, the observed instabilities in the friction coefficient after approximately 30 m of the friction path are likely attributed to the onset of local coating degradation or partial delamination. It is possible that the upper layer of the coating began to wear, resulting in unstable contact conditions and noticeable friction fluctuations. These changes are consistent with the findings of Dubois et al. [42].

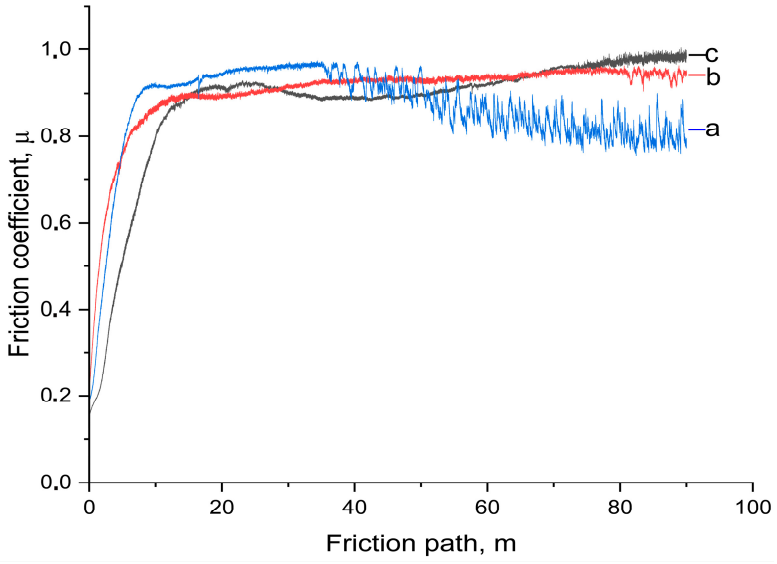

Figure 9. Changes in the coefficient of friction (μ) as a function of sliding distance (m). (**a**) 2.1 bar, (**b**) 2.3 bar, (**c**) 1.9 bar.

3.5.2. Analysis of Wear

The wear tracks after tribological tests conducted under ball-on-coating contact were examined using SEM, with the results shown in Figure 10. In Figure 10c, the wear track width of the sample ranged from 906 to 927 μm. The presence of a smooth surface within the wear track indicates signs of plastic deformation. Fine scratches and dents along the track are indicative of abrasive wear, which confirms the coating's wear resistance but also suggests partial deformation under the applied ball load. Figure 10a shows the sample obtained at an air pressure of 2.1 bar, where the wear track width ranges from 932 to 952 μm. This demonstrates the coating's resistance to mechanical loading. Moreover, despite the relatively wide wear track, the coating structure remains intact, with a high level of adhesion between the coating and the substrate; the reduced particle transfer from the coating to the ball indicates its mechanical strength and ability to withstand contact stresses. In Figure 10b, corresponding to the sample sprayed at 2.3 bar, the wear track width measures 853–902 μm. Additionally, the uneven wear may indicate structural inhomogeneity within the coating.

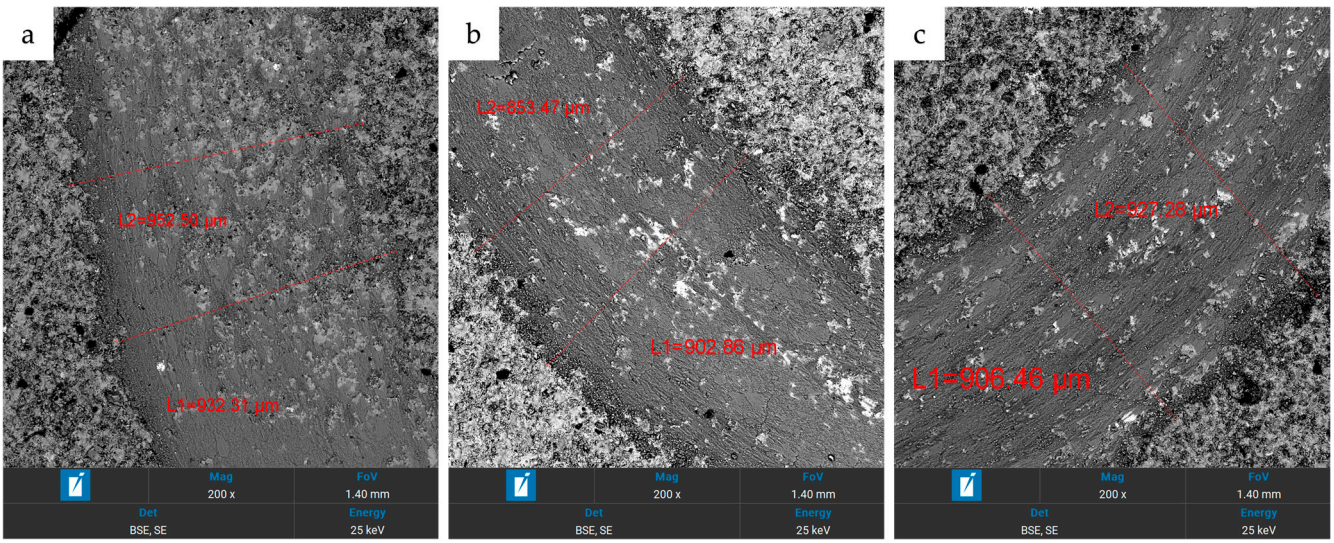

Figure 10. Wear tracks of the coatings after tribological testing involving ball-on-coating contact. (**a**) 2.1 bar, (**b**) 2.3 bar, (**c**) 1.9 bar.

According to the literature, large sintered wear particles can play a beneficial role in reducing friction. These particles act like rollers or balls between the contacting surfaces, effectively reducing the contact area and serving as a solid lubricating layer. Fleury et al. [43] observed that the formation of large cylindrical third-body particles during dry sliding of HVOF coatings is accompanied by a significant decrease in the coefficient of friction. Thus, the differences observed among samples a, b, and c can be attributed to microstructural effects: samples a and c had fine-grained structures without significant defects, ensuring a stable coefficient of friction, whereas the presence of coarse powder particles in sample b initially caused high friction, which later decreased due to the formation of beneficial third-body particles. This phenomenon aligns with general tribological principles of quasicrystalline coatings: a homogeneous quasicrystalline structure provides consistently high (yet predictable) friction, while the presence of large and heterogeneous elements may lead to variations in friction over time due to wear layer evolution. Most importantly, in the final stabilization stage, the friction coefficients of all three coatings fall within a comparable range for such materials.

3.6. Microhardness of the Coating

Figure 11 shows the Vickers microhardness (HV) values of $Al_{65}Cu_{20}Fe_{15}$-based quasicrystalline coatings obtained on U8G tool steel using the HVOF method. Before the coatings were applied, the initial microhardness of the U8G steel substrate was approximately 370 HV.

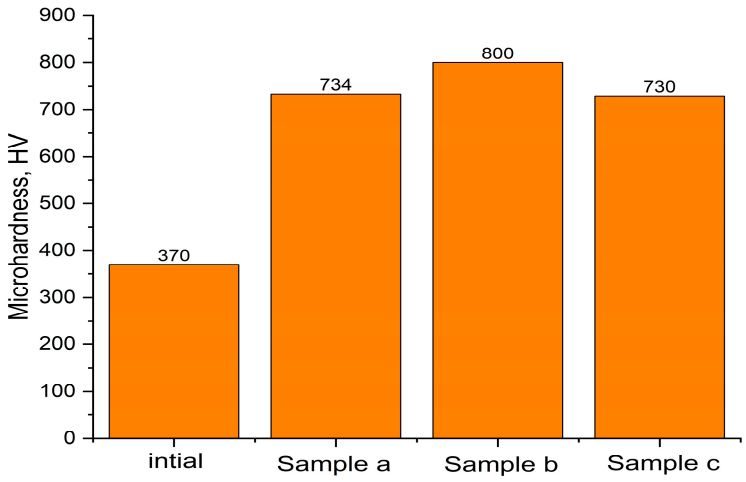

Figure 11. Vickers microhardness of $Al_{65}Cu_{20}Fe_{15}$ quasicrystalline coatings obtained by the HVOF method: a—2.1 bar, b—2.3 bar, c—1.9 bar.

The first sample a (air pressure 2.1 bar) showed a microhardness of about 734 HV. The third sample c (air pressure 1.9 bar) exhibited a value of approximately 730 HV, which is close to that of the first sample. The second sample b (air pressure 2.3 bar) showed the highest microhardness value, reaching around 800 HV. These results indicate that the coating obtained under an air pressure of 2.3 bar has the densest and most durable structure (Table 4).

In the study by Mora et al. [16], the potential of Al-Cu-Fe coatings in aerospace engineering is well demonstrated due to their hardness and anti-icing properties. The reported microhardness of the coatings is approximately 500 HV. However, this relatively low value may be attributed to insufficient optimization of spraying parameters, particularly the air pressure, which directly affects particle velocity and coating densification.

Table 4. Vickers microhardness values and statistical summary (mean and standard deviation) for the initial substrate and coated samples.

	1	2	3	4	5	Mean Hardness	Standard Deviation
Initial	370	380	360	355	375	368	10.37
Sample a	734	720	710	730	720	722.8	9.45
Sample b	780	788	798	770	800	787.2	12.54
Sample c	729	730	710	720	725	722.8	8.17

In the study by Wang et al. [25], the HVAF-sprayed Al-Cu-Fe coating demonstrates promising wear and corrosion resistance for aerospace applications, with a reported microhardness of 710 HV. However, this value remains lower than the potential of quasicrystalline Al-Cu-Fe systems (often exceeding 800 HV), likely due to suboptimal spraying conditions. The residual porosity (7.89%) and incomplete phase homogeneity particularly the interlayered soft β-phase suggest insufficient particle velocity or temperature control during deposition, limiting full densification and hardness. Further optimization of HVAF parameters (e.g., gas pressure, preheating) could enhance coating consolidation and performance.

In the present study, the microhardness of the $Al_{65}Cu_{20}Fe_{15}$ coatings reaches 800 HV, which indicates a denser and more mechanically stable structure. This improvement can be explained by the appropriate selection of air pressure during the HVOF process, which provided optimal coating formation and enhanced mechanical performance.

Its high microhardness enhances the coating's resistance to mechanical loads and wear, making it the most effective option for applications in environments with high friction forces. Additionally, the lower scatter in the microhardness values of the second sample suggests a more homogeneous structure, which further improves its performance characteristics.

4. Conclusions

Based on the analysis of the obtained results, the following conclusions can be drawn:

- SEM analysis of the microstructure revealed that increasing the air pressure to 2.3 bar leads to the formation of a denser and more uniform coating structure, characterized by low porosity and a homogeneous distribution of elements.
- These morphological features, in turn, correlated with the phase composition identified by X-ray diffraction analysis: the formation of $Al_{78}Cu_{48}Fe_{14}$ and $Al_{0.5}Fe_{1.5}$ phases, particularly at 2.3 bar, contributed to enhanced adhesion and corrosion resistance of the coating.
- Tribological tests using the "ball-on-disk" configuration confirmed that the presence of these phases positively affects the mechanical properties of the coating: the minimum wear track width (902 μm) was recorded at an air pressure of 2.3 bar. This indicates increased wear resistance and mechanical strength, which are directly linked to the phase stability and refined microstructure achieved through the optimized spraying conditions.

An air pressure of 2.3 bar is, therefore, identified as the most favorable spraying parameter for producing dense, wear-resistant, and adhesion-strong quasicrystalline coatings. These coatings show great potential for industrial applications, particularly in environments characterized by high friction, cyclic mechanical loads, and abrasive wear, such as automotive, aerospace, and tooling industries. However, further studies are recommended to evaluate the long-term durability under real-service conditions, the economic feasibility of scaling the coating process for large components, and potential cost-related limitations

associated with the production of quasicrystalline powders. The scientific contribution of this work lies in establishing a direct correlation between air pressure, phase composition, and tribological performance, offering a process route to optimize the mechanical and structural properties of Al-Cu-Fe quasicrystalline coatings. These findings contribute to advancing the development of high-performance, wear-resistant surface engineering solutions that support sustainable technological progress by extending the service life and reliability of engineering components.

Author Contributions: Conceptualization, T.G., P.S., S.K., and A.T.; investigation, S.K., D.B., S.R., S.B., and A.A.; writing—original draft preparation, S.K., S.B., and A.A.; writing—review and editing, P.S., S.K., A.T., and A.A.; visualization, S.R.; project administration, T.G.; funding acquisition, D.B. All authors have read and agreed to the published version of the manuscript.

Funding: This study is funded by the Science Committee of the Ministry of Science and Higher Education of the Republic of Kazakhstan (Grant No. AP26103943).

Institutional Review Board Statement: Not applicable.

Informed Consent Statement: Not applicable.

Data Availability Statement: The data are contained within the article.

Conflicts of Interest: Author Sherzod Kurbanbekov was employed by the company LLP "Institute of Innovative Technologies and New Materials" and Author Alibek Tazhibayev was employed by the company LLP "ALCOR". The remaining authors declare that the research was conducted in the absence of any commercial or financial relationships that could be construed as a potential conflict of interest.

References

1. Yeong-Ho, S.; Baek, S.H.; Kim, B.K.; Hwang, J.H.; Lee, J.H.; Song, G.D. Comparison of Durability and Gamma-Ray Shielding Performance of High-Velocity Oxygen Fuel Tungsten Carbide-Based Coatings on Cold-Rolled Steel Surface. *Crystals* **2025**, *15*, 21. [CrossRef]
2. Nie, H.; Li, Z.; Zhou, H.; Wu, J.; Wen, G.; Li, Y. Study on the Wear Resistance and Mechanism of HVOF-Sprayed WC10Co4Cr Coatings. *Surf. Coat. Technol.* **2024**, *494*, 131368. [CrossRef]
3. Kumar, V.; Verma, R. Effect of GNP and Laser-Surface Texturing on HVOF Sprayed WC10Co4Cr Coatings for High-Wear Resistance. *Tribol. Int.* **2023**, *178*, 108057. [CrossRef]
4. Yang, X.; Lin, H.; Chen, Y.; He, Y.; Shen, Z. Effect of AlTiN Coating Structure on the Cutting Performance of Cemented Carbide PCB Microdrills. *Coatings* **2025**, *15*, 520. [CrossRef]
5. Wang, Y.; Zhu, M.; Meng, X.; Peng, X. Effects of Laser Bionic Textures and Diamond-Like Carbon Coatings on Tribological Properties of CuAl10Fe5Ni5 Under Oil Lubrication. *Coatings* **2025**, *15*, 446. [CrossRef]
6. Rabadzhiyska, S.; Dechev, D.; Ivanov, N.; Ivanova, T.; Strijkova, V.; Katrova, V.; Valkov, S. Wear and Corrosion Resistance of ZrN Coatings Deposited on Ti6Al4V Alloy for Biomedical Applications. *Coatings* **2024**, *14*, 1434. [CrossRef]
7. Kumar, R.; Sharma, S.; Singh, J.P.; Gulati, P.; Singh, G.; Dwivedi, S.P.; Li, C.; Kumar, A.; Tag-Eldin, E.M.; Abbas, M. Enhancement in Wear-Resistance of 30MNCRB5 Boron Steel-Substrate Using HVOF Thermal Sprayed WC–10% Co–4% Cr Coatings: A Comprehensive Research on Microstructural, Tribological, and Morphological Analysis. *J. Mater. Res. Technol.* **2023**, *27*, 1072–1096. [CrossRef]
8. Mishra, B.B.; Nautiyal, H. Frictional and Wear Behavior of Cr_3C_2-NiCr Coating on AISI-304 Stainless Steel. *Adv. Mater. Process. Technol.* **2022**, *8*, 4007–4017. [CrossRef]
9. Wen, Y.; Zhang, Y.; Zhang, X.; Zhao, Z.; Yan, Q. The Tribological Behavior of Cu-Based Brake Materials against Cr_3C_2-NiCr Coated Steel Disks with Varying Roughness. *Tribol. Trans.* **2024**, *68*, 77–89. [CrossRef]
10. Ge, Y.; Xi, H.; Kong, D. Structural Evolution, Phase Transition and High-Temperature Tribological Properties of Cr_3C_2 Reinforced WC-10Co4Cr Coatings by Laser Cladding. *Ind. Lubr. Tribol.* **2025**, *77*, 582–591. [CrossRef]
11. Hao, K.; Huang, J.; Liu, H.; Wang, Z.; Qiu, Z.; Zheng, Z.; Zeng, D. Improving Thermal Shock and Oxidation Resistance of Cr_3C_2/WC-NiCr Cermet Coating by Embedding Large NiCrAlY Superalloy Particles. *Ceram. Int.* **2024**, *50*, 54737–54752. [CrossRef]

12. Zhu, L.; Soto-Medina, S.; Cuadrado-Castillo, W.; Hennig, R.G.; Manuel, M.V. New Experimental Studies on the Phase Diagram of the Al-Cu-Fe Quasicrystal-Forming System. *Mater. Des.* **2020**, *185*, 108186. [CrossRef]
13. Dubois, J.M. Properties and Applications of Quasicrystals and Complex Metallic Alloys. *Chem. Soc. Rev.* **2012**, *41*, 6760–6777. [CrossRef] [PubMed]
14. Kušter, M.; Kovač, J.; Samardžija, Z.; Komelj, M.; Semsari Parapari, S.; Podlogar, M.; Dubois, J.M.; Šturm, S. Impact of Tuned Oxidation on the Surface Energy of Sintered Samples Produced from Atomised B-Doped Al–Cu–Fe Quasicrystalline Powders. *Crystals* **2023**, *13*, 859. [CrossRef]
15. Samavat, F.; Tavakoli, M.H.; Habibi, S.; Jaleh, B.; Ahmad, P.T. Quasicrystals. *J. Alloys Compd.* **2012**, *2*, 7–14. [CrossRef]
16. Mora, J.; García, P.; Muelas, R.; Agüero, A. Hard Quasicrystalline Coatings Deposited by HVOF Thermal Spray to Reduce Ice Accretion in Aero-Structures Components. *Coatings* **2020**, *10*, 290. [CrossRef]
17. Yang, Q.; Dolatabadi, A.; Golovin, K. *Durable Icephobic and Erosion Resistant Coatings Based on Quasicrystals*; SAE Technical Paper 2023-01-1455; SAE International: Warrendale, PA, USA, 2023. [CrossRef]
18. Fleury, E.; Kim, Y.C.; Kim, J.S.; Kim, D.H.; Kim, W.T.; Ahn, H.S.; Lee, S.M. Comparative Research of the Tribological Behavior of Thermal Sprayed Quasicrystalline Coating Layers. *J. Alloys Compd.* **2002**, *342*, 321–325. [CrossRef]
19. Silva Guedes de Lima, B.A.; Medeiros Gomes, R.; Guedes de Lima, S.J.; Dragoe, D.; Barthes-Labrousse, M.G.; Kouitat-Njiwa, R.; Dubois, J.M. Self-Lubricating, Low-Friction, Wear-Resistant Al-Based Quasicrystalline Coatings. *Sci. Technol. Adv. Mater.* **2016**, *17*, 71–79. [CrossRef]
20. Rahadilov, B.K.; Kurbanbekov, S.R.; Seytov, B.; Muktanova, N.; Baltabayeva, D.E.; Katpayeva, K. Teoreticheskiye issledovaniya i resheniya optimal'nykh rezhimov protsessa termicheskogo napyleniya HVOF dlya pokrytiya Cr_3C_2-NiCr. *Vestnik NYaTs RK* **2023**, *4*, 22–31.
21. Rahadilov, B.K.; Muktanova, N.; Kakimzhanov, D.N. Vliyanie var'irovaniya rasstoyaniya napyleniya na strukturno-fazovoye sostoyaniye i mekhanotribologicheskiye svoystva pokrytiy na osnove 86WC-10Co-4Cr, poluchennykh metodom HVOF. *Vestnik NYaTs RK* **2024**, *3*, 91–104.
22. Panteleenko, F.I.; Zhen, P. Progressivnyye tekhnologii lazernoy naplavki i gazotermicheskogo napyleniya. *Liteyo i Metallurgiya* **2024**, *3*, 61–65.
23. Wolf, W.; Koga, G.Y.; Schulz, R.; Savoie, S.; Kiminami, C.S.; Bolfarini, C.; Botta, W.J. Wear and Corrosion Performance of Al-Cu-Fe-(Cr) Quasicrystalline Coatings Produced by HVOF. *J. Therm. Spray Technol.* **2020**, *29*, 1195–1207. [CrossRef]
24. Souza, T.A.; Silva, D.D.; Júnior, F.W.; Feitosa, F.R.; Gomes, R.M.; Lima, B.A. Analysis of the Surface Properties of Al–Cu–Fe–B and Al–Co–Cu Quasicrystalline Coatings Produced by HVOF. *MRS Commun.* **2021**, *11*, 873–878. [CrossRef]
25. Wang, C.; Li, Z.; Iefimov, M.O.; Mordyuk, B.N. Protection of AA2024 Alloy against Wear and Corrosion by HVAF Sprayed AlCuFe Coating. *Surf. Eng.* **2023**, *39*, 532–540. [CrossRef]
26. *GOST 1435-99*; Bars, Strips and Reels of Tool Unalloyed Steel. General Specifications. Russian Technical Standard: Moscow, Russia, 2001.
27. *ASTM G99-17*; Standard Test Method for Wear Testing with a Pin-on-Disk Apparatus. ASTM: West Conshohocken, PA, USA, 2017.
28. Karpov, I.V.; Ushakov, A.V.; Lepeshev, A.A.; Fedorov, L.Y.; Demin, V.G.; Shaikhadinov, A.A.; Karpova, O.N. Fazovyy sostav, makro- i mikrostruktury kvazikristallicheskikh poroshkov plazmokhimicheskogo sinteza. *Zh. Tekh. Fiz.* **2017**, *87*, 741–745. [CrossRef]
29. Chugunov, D.B.; Osipov, A.K.; Kalmykov, K.B.; Meshkov, L.L. Osobennosti formirovaniya kvazikristallicheskoy fazy v litykh splavakh sistemy Al–Cu–Fe. *Vestnik Moskovskogo Universiteta. Seriya 2. Khimiya* **2015**, *56*, 98–105.
30. Wang, J.; He, Y.; Yang, Z. Microstructure and Properties of Al–Cu–Fe–Ce Quasicrystalline-Reinforced 6061 Aluminum Matrix Composites after Aging. *Coatings* **2024**, *14*, 372. [CrossRef]
31. Suárez, M.A.; Esquivel, R.; Alcántara, J.; Dorantes, H.; Chávez, J.F. Effect of Chemical Composition on the Microstructure and Hardness of Al–Cu–Fe Alloy. *Mater. Charact.* **2011**, *62*, 917–923. [CrossRef]
32. Huttunen-Saarivirta, E.; Turunen, E.; Kallio, M. Influence of Cr Alloying on the Microstructure of Thermally Sprayed Quasicrystalline Al–Cu–Fe Coatings. *Intermetallics* **2003**, *11*, 879–891. [CrossRef]
33. Li, L.; Bi, Q.; Yang, J.; Fu, L.; Wang, L.; Wang, S.; Liu, W. Large-Scale Synthesis of Al–Cu–Fe Submicron Quasicrystals. *Scr. Mater.* **2008**, *59*, 587–590. [CrossRef]
34. Rukdee, S.; Friedrich, P.; Burwitz, V.; Hartner, G.; Muller, T.; Schmidt, T.; Dennerl, K. Calibration of Einstein Probe FXT-QM and FM at the PANTER X-ray Test Facility. *Proc. SPIE Int. Conf. Space Opt.—ICSO* **2023**, *12777*, 1441–1457. [CrossRef]
35. Shalaeva, E.V.; Selyanin, I.O.; Smirnova, E.O.; Smirnov, S.V.; Novachek, D.D. Deformation Behavior and Structure of the i-Al–Cu–Fe Quasicrystalline Alloy in the Vicinity of a Nanoindenter Imprint. *Phys. Solid State* **2018**, *60*, 307–314. [CrossRef]
36. Tan, C.W.; Djuansjah, J.R.P.; Idris, M.H.; Ali, W.F.F. Characterisation of $Al_{65}Cu_{20}Fe_{15}$ Quasicrystal Alloy Synthesised via In-situ Casting under Standard Room Ambient and Argon Enriched Atmosphere. *Int. J. Curr. Res. Sci. Eng. Technol.* **2018**, *1*, 280. [CrossRef]

37. Babilas, R.; Młynarek, K.; Łoński, W.; Łukowiec, D.; Kądziołka-Gaweł, M.; Czeppe, T.; Temleitner, L. Structural Characterization of $Al_{65}Cu_{20}Fe_{15}$ Melt-Spun Alloy by X-ray, Neutron Diffraction, High-Resolution Electron Microscopy and Mössbauer Spectroscopy. *Materials* **2020**, *14*, 54. [CrossRef]
38. Ovchinnikov, A.; Smetana, V.; Mudrin, A.V. Metallic alloys at the edge of complexity: Structural aspects, chemical bonding and physical properties. *J. Phys. Condens. Matter* **2020**, *32*, 243002. [CrossRef]
39. Erkisi, A.; Surucu, G. The Investigation of DO3-Type Fe_3M (M = Al, Ga, Si and Ge) Full-Heusler Alloys within First Principles Study. *Politeknik Dergisi* **2018**, *21*, 927–936. [CrossRef]
40. Rakhadilov, B.; Satbayeva, Z.; Ramankulov, S.; Shektibayev, N.; Zhurerova, L.; Popova, N.; Sagdoldina, Z. Change of 0.34 Cr-1Ni-Mo-Fe Steel Dislocation Structure in Plasma Electrolyte Hardening. *Materials* **2021**, *14*, 1928. [CrossRef] [PubMed]
41. Pougoum, F.; Martinu, L.; Klemberg-Sapieha, J.E.; Savoie, S.; Schulz, R. Wear Properties of Fe_3Al-Based HVOF Coatings Strengthened with In-Situ Precipitated Nitride and Boride Particles. *Surf. Coat. Technol.* **2016**, *307*, 109–117. [CrossRef]
42. Dubois, J.M.; Belin-Ferré, E. Friction and Solid-Solid Adhesion on Complex Metallic Alloys. *Sci. Technol. Adv. Mater.* **2014**, *15*, 034804. [CrossRef]
43. Fleury, E.; Kim, Y.C.; Kim, J.S.; Ahn, H.S.; Lee, S.M.; Kim, W.T.; Kim, D.H. Sliding Friction and Wear Behavior of Al–Ni–Co–Si Quasicrystalline Coatings Deposited by the High-Velocity Oxy-Fuel Spraying Technique. *J. Mater. Res.* **2002**, *17*, 492–501. [CrossRef]